Astronomy & Astrophysics manuscript no. DrArc
October 28, 2015
© ESO 2015

arXiv:1510.07948v1 [astro-ph.SR] 27 Oct 2015

Mid-IR spectra of Pre-Main Sequence Herbig stars: an explanation for the non-detections of water lines

Antonellini[1], S., Kamp, I.[1], Lahuis, F.[2], Woitke, P.[3], Thi, W.-F.[4,5], Meijerink, R.[6], Aresu, G.[1,7], Spaans, M.[1], Güdel, M.[8], and Liebhart, A.[8]

[1] Kapteyn Astronomical Institute, Postbus 800, 9700 AV Groningen, The Netherlands
e-mail: antonellini@astro.rug.nl
[2] SRON Netherlands Institute for Space Research, P.O. Box 800, 9700 AV Groningen, The Netherlands
[3] St. Andrews University, School of Physics and Astronomy
[4] Univ. Grenoble Alpes, IPAG, F-38000 Grenoble, France CNRS, IPAG, F-38000 Grenoble, France
[5] Max-Planck-Institut für extraterrestrische Physisk, Giessenbachstrasse 1, 85748 Garching, Germany
[6] Leiden Observatory, Leiden University, PO Box, 2300 RA Leiden, The Netherlands
[7] INAF, Osservatorio Astronomico di Cagliari, via della Scienza 5, 09047 Selargius, Italy
[8] University of Vienna, Department of Astronomy, Türkenschanzstrasse 17, 1180 Vienna, Austria

ABSTRACT

Context. The mid-IR detection rate of water lines in disks around Herbig stars disks is about 5%, while it is around 50% for disks around TTauri stars. The reason for this is still unclear.
Aims. In this study, we want to find an explanation for the different detection rates between low mass and high mass pre-main-sequence stars (PMSs) in the mid-IR regime.
Methods. We run disk models with stellar parameters adjusted to spectral types B9 through M2, using the radiation thermo-chemical disk modeling code ProDiMo. We produce convolved spectra at the resolution of Spitzer IRS, JWST MIRI and VLT VISIR spectrographs. We apply random noise derived from typical Spitzer spectra for a direct comparison with observations.
Results. The strength of the mid-IR water lines correlates directly with the luminosity of the central star. We explored a small parameter space around a standard disk model, considering dust-to-gas mass ratio, disk gas mass, mixing coefficient for dust settling, flaring index, dust maximum size and size power law distribution index. The models show that it is possible to suppress the water emission; however, current observations are not sensitive enough to detect mid-IR lines in disks for most of the explored parameters. The presence of noise in the spectra, combined with the high continuum flux (noise level is proportional to the continuum flux), is the most likely explanation for the non detections towards Herbig stars.
Conclusions. Mid-IR spectra with resolution higher than 20000 are needed to investigate water in protoplanetary disks. Intrinsic differences in disk structure, e.g. inner gaps, gas-to-dust ratio, dust size and distribution, and inner disk scale height, between Herbig and TTauri star disks are able to explain a lower water detection rate in disks around Herbig stars.

Key words. Protoplanetary disks - line: formation - Stars: pre main-sequence: TTauri, Herbig - circumstellar matter - Stars: individual (HD 100546, HD 97048, HD 163296, HD 142666, HD 135344B, RY Tau, RY Lup, DN Tau, CY Tau, DO Tau)

1. Introduction

Water has been detected successfully towards many T Tauri disks in the IR (Salyk et al., 2008; Carr & Najita, 2008; Pontoppidan et al., 2010a,b; Bergin et al., 2010; Hogerheijde et al., 2011; Riviere-Marichalar et al., 2012). Contrary, disks around Herbig stars do not show warm water lines both in mid-IR (15.17, 17.22, 29.85 μm blends from Pontoppidan et al., 2010a), and in the near-IR (2.9345 μm ro-vibrational lines from Fedele et al., 2011). Far-IR water lines have been detected towards the Herbig star HD 163296 (Meeus et al., 2012; Fedele et al., 2012); tentative detections are reported towards other targets such as HD 31648 (63 μm), HD 97048 and HD 100546, but the blend with the CH^+ at 90 μm and 179.5 μm prevent a firm claim for the detection of water at this wavelength (Meeus et al., 2012). Finally six successful detections of the OH molecule have been reported from the Keck II NIRSPEC instrument towards AB Aur and MWC 758 (Mandell et al., 2008), and from CRIRES towards V380 Ori, HD 250550, HD 259431, HD 85567 (Fedele et al., 2011).

Several possible explanations have been considered for the non detections of water and other molecular features towards Herbig stars: veiling due to stronger continuum (Pontoppidan et al., 2010b), difference in dust content of the emitting layers (due to a different dust-to-gas mass ratio or settling, Meijerink et al., 2009), different efficiency in the heating of the surface layers, a difference in the chemistry between Herbig and T Tauri disks, the transitional nature of the observed disks. The inner disk physical conditions seems to be independent from the mass of the central star (Salyk et al., 2008; Mandell et al., 2008), since the OH and water lines are consistent with the same gas temperature and location of the emitting regions of both T Tauri and Herbig stars. We know that some disks around Herbig stars are transitional, and in some of these OH, CO-rovibrational and OI lines have been detected (e.g. HD 100546 Liskowsky et al., 2012). However, in some cases the inner cavity is not totally gas depleted, and transitions as the CO-rovibrational band at 5 μm are still detectable

(Salyk et al., 2009). The last hypothesis, the role of FUV radiation field in photodissociating water in the inner disk seems supported by NIRSPEC & CRIRES observations of OH (respectively, Mandell et al., 2008; Fedele et al., 2011). Multi-epoch Spitzer spectra of the variable star EX Lup (Banzatti et al., 2012) support the idea that photochemistry must be responsible for organics depletion, enhanced OH column density and reduced water column density.

Modeling of Herbig stars performed with the radiation thermo-chemical code ProDiMo (Woitke et al., 2011) suggests that disks around Herbig Ae stars are not dry, and are still able to emit far-IR lines. The presence of the gaseous reservoir in the outer disk is due to an interplay between photodissociation and photodesorption. Due to this interplay, water vapour is present even in disks around bright stars (as the Herbigs, that have stronger FUV flux), but the water ice reservoir is less extended with respect to the case of disks around low mass stars (van Dishoeck et al., 2014). The inner disk water vapour reservoir is radially more extended in disks around earlier type stars (higher effective temperature, $T_{\rm eff}$, Du & Bergin, 2014).

In a previous work (Antonellini et al., 2015) we investigated the effects of different disk parameters on the chemistry and water spectroscopy in the mid- and far-IR. We identified key parameters affecting the continuum opacity and the gas content of the disk as drivers of the mid- and far-IR lines. The explanation for low detection rate of the far-IR water lines with Herschel/HIFI is likely sensitivity; the observations were often not deep enough.

In this work, we focus on the difference between low and high mass PMSs. We searched for factors which can be responsible for the absence of mid-IR water lines in disks around Herbig stars, comparing the results with what we find for T Tauri and intermediate mass PMS. We model here a different central star, inner disk properties and instrumental properties. In Section 2, we describe the code and modeling approach. In Section 3, we report our results. In Section 4, we discuss the results and finally in Section 5, we present our conclusions.

2. Modeling

We perform modeling of protoplanetary disks using the radiation thermo-chemical code ProDiMo ("Protoplanetary Disk Model") including X-ray photoprocesses (Woitke et al., 2009; Aresu et al., 2011). The code computes self consistently the chemistry (steady state) with the heating/cooling balance. Heating processes implemented include PAH/photoelectric heating, C photoionization, H_2 photodissociation, formation heating and collisional de-excitation, cosmic rays heating, viscous heating, pumping by OH photodissocation, H_2 pumping by formation on dust grains, and chemical heating and several others. Cooling processes occur through more than 10000 atomic/molecular emission lines. Finally, gas and dust thermalization is also taken into account. Other features include a computation of the photo-rates using detailed cross-sections and an extension of the collisional partners for water (Kamp et al., 2010), a soft-edge description of the outer disk, the PAH ionization balance and heating/cooling, UV fluorescence pumping, a parametric description of settling (Woitke et al., 2011).

We computed here the detailed statistical equilibrium of a subset of 500 ro-vibrational levels, from the complete set (Tennyson et al., 2001; Barber et al., 2006), which includes up to 411 o-H_2O and 413 p-H_2O ro-vibrational levels (rotational levels up to $J = 25$; projections up to $K_{\rm a,c} = 18$; vibrational levels up to $v_1 = 2$, $v_2 = 2$, $v_3 = 1$). The study here focuses on the 12 μm series of lines observed from the ground by Pontoppidan et al. (2010b) and described also in our previous work (Antonellini et al., 2015). In addition, we consider the blends centered at 15.17 μm observed by Spitzer IRS and reported in Pontoppidan et al. (2010a). Our line fluxes are derived from level populations computed through vertical escape probability. This approach has been used also in our previous work (Antonellini et al., 2015) and it provides line fluxes trustable within a factor two from a more computationally expensive detailed radiative transfer. The transitions we consider in this work are from very warm gas layers, and have $E_{\rm up}$ larger than 500 K. The transitions contributing to the 12.407 μm blend have $E_{\rm up} > 3000$ K, while the lines contributing to the 15.17 μm blend have $E_{\rm up} > 2700$ K.

2.1. Central star

For the basic model, we use the same standard disk as in our previous work on TTauri stars (properties are described in Table 2). We then consider different central star spectra corresponding to real observed PMS targets, including the non photospheric contributions due to accretion[1] and X-rays. The spectra are built constraining the photometric observations in the optical and the UV by fitting $T_{\rm eff}$, $R_{\rm V}$, $p_{\rm UV}$, $f_{\rm UV}$, using literature values for the distance and $M_{\rm star}$ (Woitke et al. submitted). We use the Kurucz and Phoenix stellar atmosphere libraries (Husser et al., 2013; Murphy & Meiksin, 2004), and the high energy spectra merging IUE, HST and FUSE observations for the FUV, and XMM Newton, Chandra for the X-rays after a post-processing described in Dionatos et al. in prep. FUV data for the stars we considered are in Appendix C.

The 10 different central stars we consider are based on observed available data (Table 1). The sample includes spectral types from M2 to B9 in order to probe the effects of a different photospheric temperature and luminosity, but also different non photospheric contributions. The input spectra used for the code are the result of the merging of three spectral regions: photospheric (optical, near-IR, photospheric UV), UV excess, X-rays. Every of these contributions has its own luminosity: $L_{\rm star}$ is the photospheric luminosity, $L_{\rm UV}$ is the UV excess (from 3300 Å up to 1150 Å, variable from source to source), $L_{\rm X}$ is the X-ray luminosity (from 5 Å up to 35 Å, variable from source to source). We check the consistency of the fitted stellar parameters with the Siess' track isochrones (Siess et al., 1999)[2], taking the published age of the star and the mass, and verifying the consistency with the expected $T_{\rm eff}$, $L_{\rm star}$ and $R_{\rm star}$.

2.2. Parameter space exploration of a disk around a typical Herbig star

We build also a small parameter series, exploring a subset of disk properties listed in Table 2: scale height radial power law index β, dust-to-gas mass ratio, disk gas mass, scale height of the disk at the inner disk radius, inner disk radius, mixing coefficient for the dust settling (accordingly to the settling prescription from Dubrulle et al., 1995), dust size distribution power law

[1] In this work as in the previous, we did not treat the presence of UV excess consistently with the presence of viscous heating. Our disks are passive. FUV excess is considered as an extra UV radiation field emitted isotropically from the central star.

[2] http://www.astro.ulb.ac.be/ siess/pmwiki/pmwiki.php/WWWTools /Isochrones

Table 1: Central star properties

Star	Sp.Type[(*)]	M_{star} [$M_\odot$]	d [pc]	A_V [mag]	R_{star} [$R_\odot$]	T_{eff} [K] (fit)	L_{star} [$L_\odot$] (fit)	L_{FUV}/L_{star}	L_{X-ray}/L_{star}
HD 100546	B9V	2.50[(1)]	103±6[(2,26)]	0.36[(20)]	1.9[(Siess)]	11412	42.3	0.226	$9.779\cdot10^{-7}$
HD 97048	A0	2.50±0.20[(3,25,27)]	158[(25)]	1.24[(1)]	2.12[(25)]	10000	33.5	0.151	$4.345\cdot10^{-7}$
HD 163296	A4 (A1Ve)	2.47[(5)]	122.0[(4,25,26,27)]	0.5[(19)]	2.3±0.1[(19)]	8907	38.3	0.088	$5.345\cdot10^{-7}$
HD 142666	A8V	1.6[(6)]	145±43[(27)]	0.8[(6)]	1.483[(21)]	7297	6.4	0.030	$2.114\cdot10^{-6}$
HD 135344B	F5V (F8V)	$1.70^{+0.2(8)}_{-0.1}$	140.0[(25,26,27)]	0.4[(17)]	2.2[(25)]	6950	8.1	0.007	$2.871\cdot10^{-5}$
RY Tau	F8V (F8Ve-K1IV-Ve)	2.24±0.07[(24)]	140.0[(9)]	2.2[(9)]	2.9[(9)]	5496	10.9	0.067	$5\cdot10^{-4}$
RY Lup	G0V	1.38[(11)]	120±35[(28)]	2.48	1.67[(11)]	5200	2.6	0.221	$9.845\cdot10^{4}$
DN Tau	K6V	0.65±0.05[(12)]	140.0[(14)]	$\simeq$ 0.5[(12)]	1.9±0.2[(12)]	3904	0.8	0.002	$6.946\cdot10^{-4}$
CY Tau	M2V (M1.5)	0.48±0.05[(24)]	140.0[(14)]	0.1[(16,24)]	1.4[(16)]	3628	0.4	0.003	$7.482\cdot10^{-5}$
DO Tau	M6 (GV:e)	0.56±0.05[(24)]	140.0[(14,16)]	2.64[(24)]	2.4[(16)]	3777	1.3	0.090	$1.07\cdot10^{-4}$

Notes. For all stars, we assumed $R_V = 3.1$. The radius for HD100546 has been retrieved from the Siess evolutionary track (Siess et al., 1999).

References. (*) http://simbad.u-strasbg.fr/simbad/sim-fid; (1) van den Ancker et al. (1997), (2) Perryman et al. (1997), (3) van Leeuwen (2007), (5) Tilling et al. (2012), (6) Garcia Lopez et al. (2006), (8) Müller et al. (2011), (9) López-Martínez & Gómez de Castro (2014), (11) Manset et al. (2009), (12) Donati et al. (2013), (14) Luhman et al. (2010), (16) Hartigan et al. (1995), (17) Carmona et al. (2014), (19) Ellerbroek et al. (2014), (20) Ardila et al. (2007), (24) Bertout et al. (2007), (25) Maaskant et al. (2014), (26) McJunkin et al. (2014), (27) van Boekel et al. (2005), (28) Fedele et al. (2013)

index, dust grains maximum size. Each model contains all the quantities fixed and equal to our standard model ones, except the ones indicated in Table 2. A more detailed description of the previous disk properties can be found in Antonellini et al. (2015). This kind of exploration allows us to disentangle effects of single parameters on disks irradiated by a central Herbig star. In this small parameter series, the disk is irradiated by a typical Herbig star (2.2 $M_\odot$, 32 $L_\odot$, 8600 K). The disk considered is the same as the standard disk model of our previous work (Antonellini et al., 2015), with the exception of the inner radius, which is computed consistently with the sublimation temperature of the dust (R_{in} = 0.365 au; Table 2).

3. Results

3.1. Series 1: Different central star

The general trend is shown in Fig. 1, where the flux of the 12.407 μm water blend is plotted for our models with different central star. The mid-IR transitions get stronger with increasing photospheric temperature, although the progression is not linear. This can be explained by a combination of different stellar spectrum properties (e.g. hardness of the X-ray component, color of the FUV excess), that can affect the heating/cooling and or water abundance in the inner reservoir in a complex manner. In a previous study, Aresu et al. (2012) explored the effect of X-rays on far-IR water lines, finding that the 179 μm flux grows with L_X independently from the UV. The situation becomes more complex analyzing transitions produced in the inner disk. There is an L_{UV} threshold above which X-ray affects the far-IR water line fluxes. In our previous work (Antonellini et al., 2015), we found that mid-IR transitions originate from regions in which water is produced by thermally activated channels and depleted by photodissocation. The spectroscopy in this region is affected by FUV radiation. Overall, the line flux of the mid-IR lines correlates with the stellar bolometric luminosity (Fig. 2), and it is correlated with the FUV and uncorrelated with X-ray luminosities (blue and magenta symbols in the same plot). However the sample of stellar spectra studied is too small to go into a deeper analysis.

The theoretical Spitzer spectra (Fig. 3) predict that the earliest spectral types have a richer mid-IR spectrum. A zoom into the 12 μm region shows that the trend is not only dictated by the

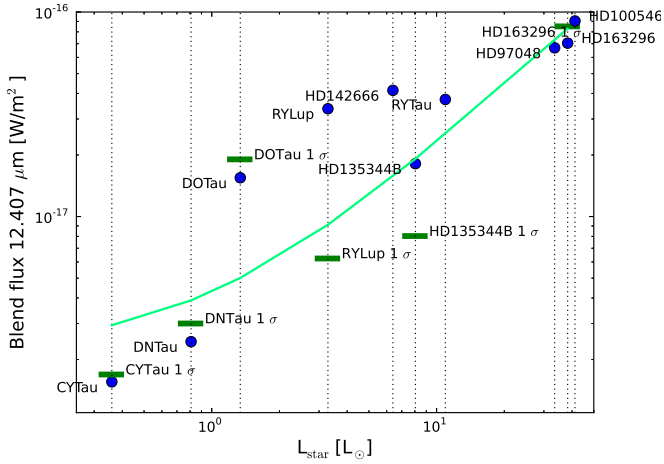

Fig. 1: Line fluxes and luminosities from the central star versus effective temperature for Spitzer 12.407 μm blend. The blue dots are the line fluxes of the models for the different central stars. The stars mark, the luminosities in the different wavelength bands. Detection limits for Spitzer IRS observations towards the same central star disks are plotted as thick green dashes (see Appendix A). Light green curve is a fits to the sensitivity limits. The central stars are labeled with the name reported in column 1 of Table 2.

spectral type: DN Tau (K6V) and CY Tau (M2V) are the only two objects with L_{star} < 1 $L_\odot$ (and FUV less than 5% of the bolometric), and they show weaker mid-IR water lines. For example the M2V spectral type star (L_{star} = 0.4 $L_\odot$) 12.407 μm flux is a factor 17 weaker than the M6 case (L_{star} = 1.3 $L_\odot$). This suggests again that the bolometric luminosity is the real driving force behind the mid-IR spectroscopy.

From Spitzer IRS observations towards the central stars we modeled (blue dots with thick green dashes in Fig. 1), we find that the sensitivity anticorrelates with the stellar luminosity, indicating that observations around brighter stars are less sensitive. The sensitivity limit for HD 163296 (Spectral type A4) in Spitzer spectra is very close to our standard disk model generated for the spectral type A4 (HD 163296 in Fig. 1). The disk structure around this Herbig star has been robustly fitted by Tilling et al. (2012) using multi-wavelength observations; it is very similar to our standard disk model. This may point to the fact that obser-

Table 2: Herbig disk grid

Standard disk model parameters		
Parameter	Symbol	Value
Grid points	N_{xx}/N_{zz}	70×70
Outer radius	R_{out} [au]	300
Surface density power law index	ϵ	1.0
Minimum dust size	a_{min} [μm]	0.05
Tapering-off radius	R_{taper} [au]	200
Chemical Heating	-	0.2
Settling description	-	Dubrulle
Cosmic ray ionization rate	ζ_{CRs} [s^{-1}]	1.7×10^{-17}
distance	d [pc]	140
Turbulence viscosity coefficient	α_{vis} [-]	0
Dust properties	-	astrosilicates(1)
Disk parameters varied in the series of models irradiated by a typical Herbig star(2)		
Parameter	Symbol	values
Flaring power law index	β	-0.8, -0.5, -0.1, 0.0, 0.8, 0.85, 0.9, 0.95, 1.0, 1.05, 1.1, **1.13**, 1.15, 1.2, 1.25
Dust-to-gas mass ratio	d/g	0.001, **0.01**, 0.1, 1, 10, 100
Disk gas mass	M_{gas} [$M_\odot$]	10^{-5}, 10^{-4}, 0.001, **0.01**, 0.05, 0.1
Inner disk scale height (at $R = R_{in}$)	H_0 [au]	1.8(-3), 4.4(-3), 9.0(-3), **1.76**(−**3**), 3×10^{-2}, 0.1
Inner radius	R_{in} [au]	0.1, **0.365**, 0.5, 1.0, 5.0, 10.0, 15.0, 20.0, 25.0, 30.0
Mixing coefficient	α_{set}	10^{-5}, 10^{-4}, 0.001, 0.01, **0.05**, 0.1
Dust power law index	a_{pow}	2.0, 2.5, 3.0, **3.5**, 4.0, 4.5
Dust maximum size	a_{max} [μm]	250, 400, 500, 700, **1000**, 2000, 5000, 10^4, 10^5
Elemental abundance of O	$\Delta Y_O = Y_{O,i} - Y_{O,standard}$	-0.5, -0.4, -0.3, -0.2, -0.1, **0.0**, 0.1, 0.2, 0.3, 0.4, 0.5

Notes. Bold numbers refer to standard model values. In parenthesis are shown the orders of magnitude for the values of the models with different scale height. (1) Draine & Lee (1984); (2) M_{star} = 2.2 $M_\odot$, L_{star} = 32 $L_\odot$, T_{eff} = 8600 K

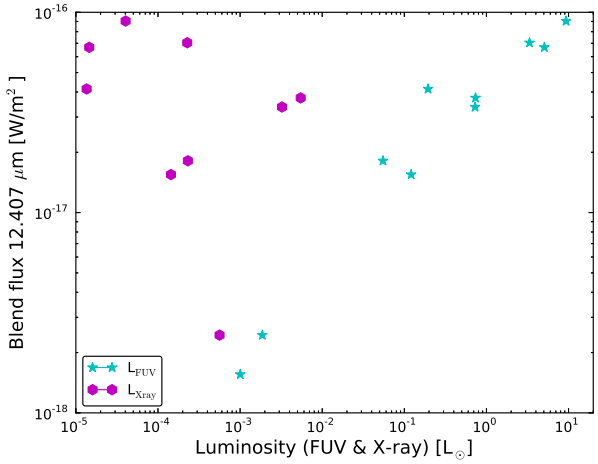

Fig. 2: Line fluxes for Spitzer 12.407 μm blend versus L_{FUV} (stars cyan) and L_X (magenta exagons).

vations for this object were simply not deep enough to detect the mid-IR water lines.

The modelled IRS spectra for different central stars seem to disagree with the observations towards a large sample of Herbig stars, whose spectra are featureless (Pontoppidan et al., 2010a). The reason for the disagreement between observations and modeling can be twofold: either the structure of Herbig disks is different from TTauri disks, or instrumental effects affect differently the spectra of these two types of PMS disks. In the next two paragraphs, we test the first hypothesis comparing the result of modelling with observations, and then we apply instrumental characteristics to test the second hypothesis.

3.2. Series 2: Rockline displacement effect

The results from the standard disk irradiated by a different central star contain an inconsistency (since we wanted to isolate the effect of a changing central star from that of disk changes). The inner disk radius remains fixed at 0.1 au. Taking instead 1500 K as sublimation temperature for the dust (silicates) as adopted in Min et al. (2011), Fig. 4 shows how the disk inner radius is shifted outward for earlier type stars. For T Tauri stars with $L_{star} < 1.5\ L_\odot$, the inner radius is even truncated inward of 0.1 au.

In order to study the impact of a disk truncated by dust sublimation, we ran a series of models considering different disk inner radii and another one with different scale heights using always the same central star, a typical Herbig star (see Notes of Table. 2). The larger inner disk radii produce a suppression of the whole mid-IR spectrum, in particular if the gap extends beyond 10 au (Fig. 5). For inner radii less than 1.0 au, the Spitzer features become weaker again, due to a geometrical effect: the line is emitted further inward and the total emitting area becomes smaller. Increasing the scale height of the same disk, will strongly reduce the continuum opacity. As a consequence, the water ice reservoir is totally depleted and the water vapor reservoir is radially more extended (in particular the innermost one). The emitting water column density increases and mid-IR water lines become stronger. This is particularly true for disks with a scale height larger than 2×10^{-3} au at $R = 0.1$ au.

The true rockline displacement is limited to tenth of au, and the lowering in scale height is about a factor 2 with respect to our standard disk for the brightest Herbig star we considered (Fig. 4). In order to suppress the Spitzer water line emission, it would be necessary to open a gap larger than 5-10 au and contract the disk vertically by more than a factor 2. In particular, the 15.17 μm blend drops below the typical sensitivity

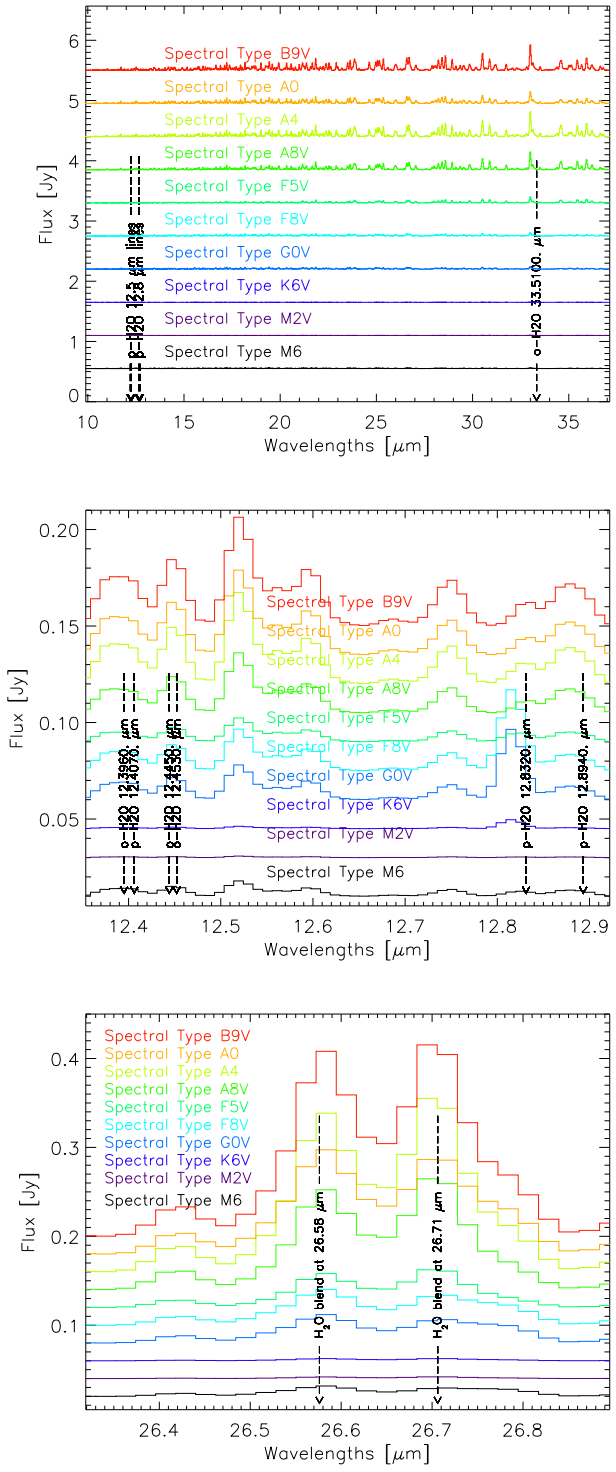

Fig. 3: Theoretical Spitzer SH/LH spectra (convolved at R = 600 and rebinned) for models with different central stars; full continuum subtracted spectrum, artificially shifted for all the models (top), zoom on the 12 μm region (middle), zoom on the 26.5 μm region (bottom).

range we defined for Spitzer IRS observations of Herbig stars (**8×10**$^{-17}$**-8×10**$^{-18}$ W/m^2) for $R_{\rm in}$ > 20 au and H_0 smaller than 9×10^{-3} au. This numerical test rules out that a simple difference in the disk structure is responsible for the water non-detections towards Herbig disks.

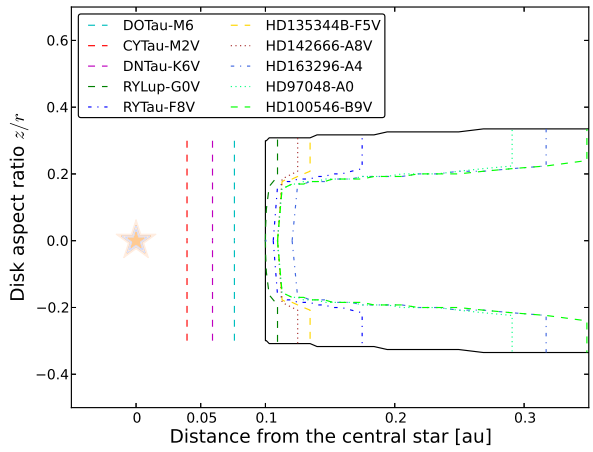

Fig. 4: Rockline position for the disks around different central stars. The thick black line indicates the disk contour at the gas density of 5·10^3 cm^{-3} for all our disk models, we consider it as delimitation of our disk, due to the fact that the erosion happens at more then 4 disk scale heights. The different color and line styles delimitate the contours of the disk with $T_{\rm dust}$ = 1500 K assumed as sublimation temperature of silicates, upward and inward of this contour the dust is sublimate, and the disk is truncated. It describes the effective extension of the disk accordingly to the dust sublimation temperature. For late type stars disk temperatures are too low and the contour is replaced by a vertical line, that indicates the distance from which the dust in thermal equilibrium should be photoevaporated. The position of the central star is indicated by the star symbol.

3.3. Series 3: Extended parameter space exploration

For a direct comparison with Spitzer observations of Herbig disks, we expand the parameter space exploring also the dust-to-gas mass ratio, the flaring index, the gas mass, the C/O ratio, the settling (through the $\alpha_{\rm set}$ turbulent coefficient from Dubrulle et al., 1995), and the dust maximum size and power law distribution ($a_{\rm pow}$), around the typical central Herbig star (Sect. 2). Fluxes extracted for mid-IR water blends at 15.17 μm (Pontoppidan et al., 2010a) are compared to the results from our series of models. As mid-IR continuum tracer, we used the same ratio considered in our previous work (13.5/30 μm, Antonellini et al., 2015). Fig. 7 shows the same plot as for the T Tauri disk model series (Fig. 13 top panel, Antonellini et al., 2015). In our previous paper we showed that the transitions contributing to this blend behave in the same manner as our representative 12.407 μm line, and the same holds for the blends at 17 and 29 μm. Any conclusion on this blend will be representative of the entire mid-IR water spectrum.

The standard Herbig star disk, which is the base model of the parameter space exploration (Table 2) is located in the central part of Fig. 7, where all the model series intersect. We notice that a certain fraction of the targets and of our parameter space study is below the range of detection threshold deduced from the sensitivity limits reported in Fig. 1. Part of the targets that would be detectable at 140 pc are too distant, and the exposure time length was not optimal for these objects. The fact that our typical Herbig model is close to the sensitivity range in Fig. 7 suggests that instrumental factors may have played an important role in the chance of detecting water lines in Spitzer IRS observations.

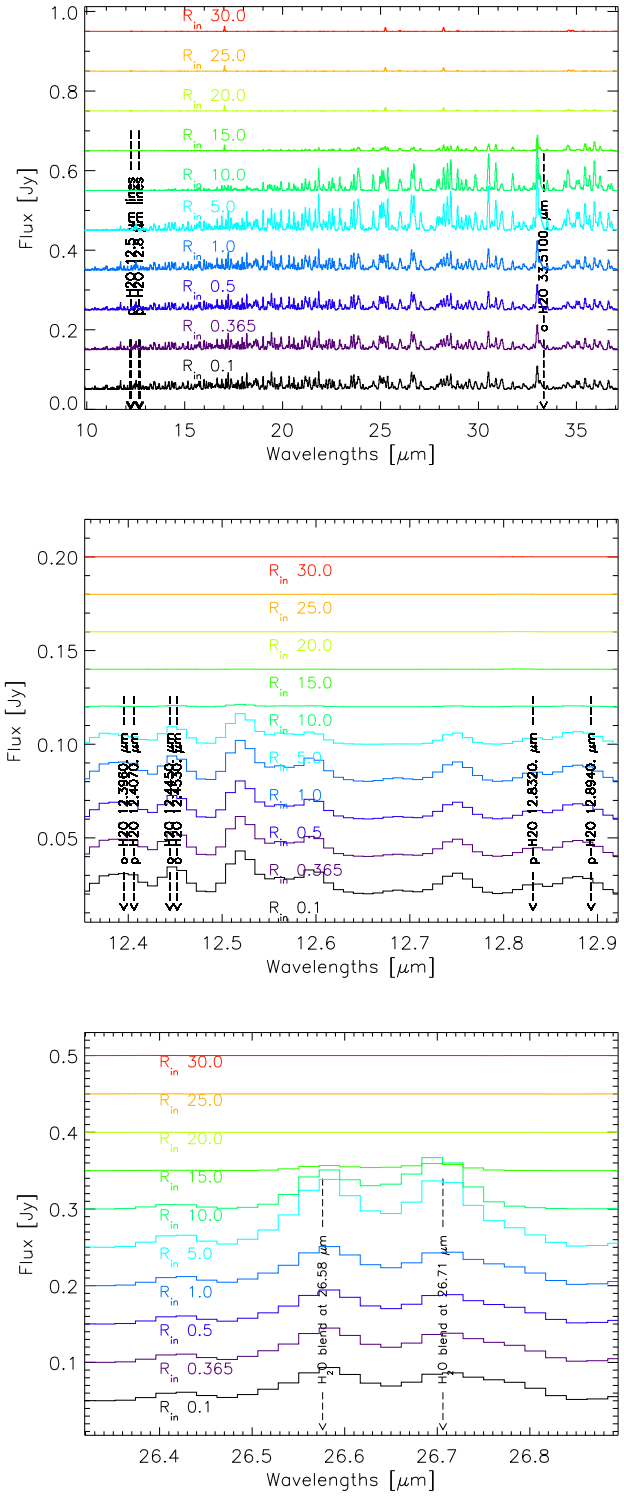

Fig. 5: Continuum subtracted theoretical Spitzer spectra for $R_{\rm in}$ variation, artificially shifted, convolved at the resolution of $R = 600$ and rebinned. Second plot is a zoom of the complete spectrum on the 12 μm region. Third plot is a zoom on the 26.5 μm region.

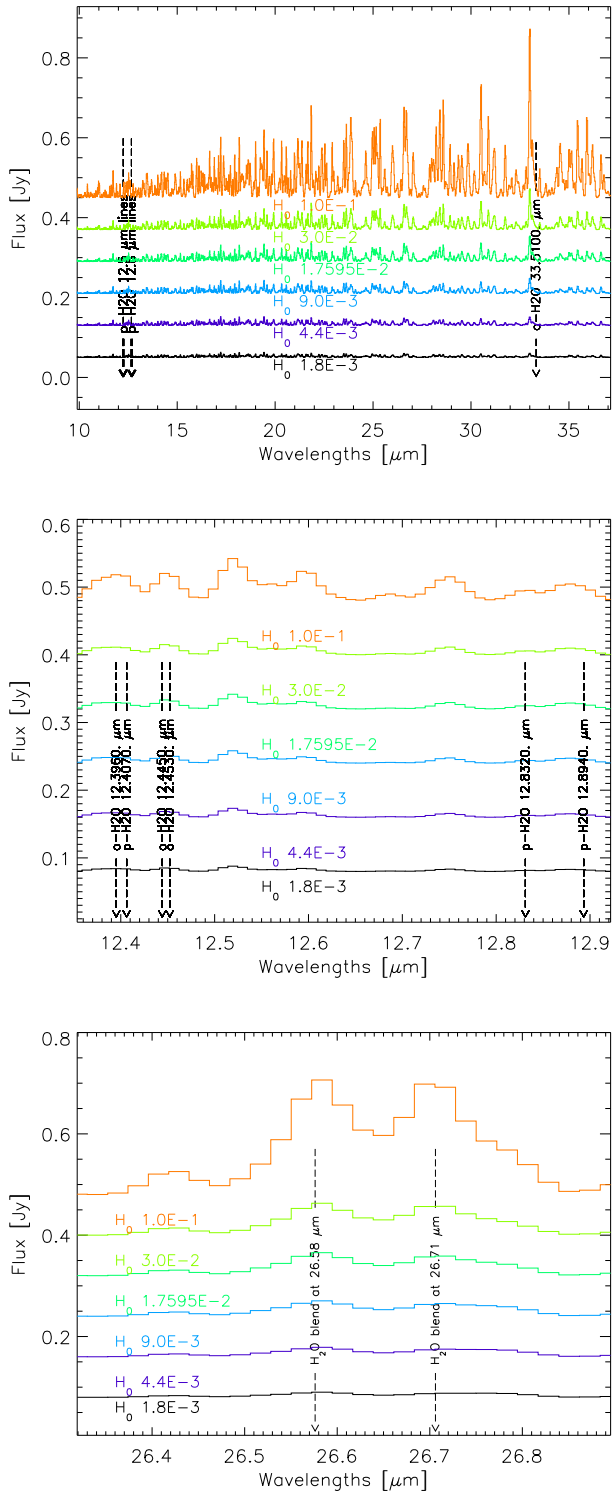

Fig. 6: Continuum subtracted theoretical Spitzer spectra for H_0 variation, artificially shifted, convolved at the resolution of $R = 600$ and rebinned. Second plot is a zoom of the complete spectrum on the 12 μm region. Third plot is a zoom on the 26.5 μm region.

3.4. Instrumental effects

The previous discussion is based on spectra unaffected by instrumental noise. Observations of water towards disks in the mid-IR wavelength range have been performed with the Spitzer Space Telescope and from the ground with the VLT (e.g. Pontoppidan et al., 2010b). The future of near- and mid-IR water studies is JWST. In order to take into account instrumental effects, we rebinned our oversampled modeled spectra and ap-

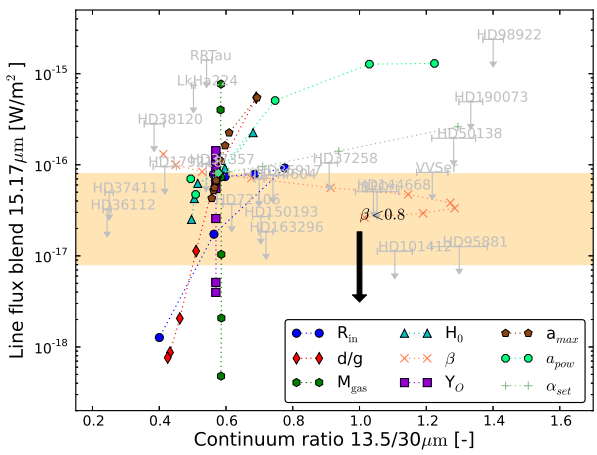

Fig. 7: Herbig parameter space for the water line blend at 15.17 μm. In the plot the data points (all upper limits, in grey) are from (Pontoppidan et al., 2010a). All the fluxes are scaled to 140 pc. The shaded yellow area contains the range of sensitivity we retrieved from Spitzer spectra of Herbig stars HD 135344B and HD 100546. All the fluxes of the disks considered are scaled to 140 pc. The trend of disks flatter than $\beta = 0.8$ is shown with a black arrow, since too flat models will be self-shadowed, and the derived mid-IR color cannot be compared in a trustable manner with observations, in which the shadowing can be partial due to a more complex disk structure.

plied random noise effects (see Appendix B) to the convolved spectra (Spitzer $R = 600$, Houck et al., 2004).

The rebinning procedure and the application of the random noise to the central stars models (Fig. 8) have the effect to suppress the water line fluxes in the mid-IR spectra. The effect is particularly dramatic for the earlier type stars, since they show a stronger continuum, and so a stronger noise. The possibility to use space or ground based instruments (in the mid-IR windows) with larger spectral resolution and sensitivity, would increase the detections of spectral features in the mid-IR towards both Herbig and T Tauri stars.

Theoretical spectra of the global mid-IR spectrum and some zoom on two regions (12.4 μm and 26.6 μm) convolved at the resolutions of Spitzer IRS (Houck et al., 2004), JWST MIRI (Clampin, 2011) and VISIR on VLT (Lagage et al., 2000) (see Appendix B), are plotted in Fig. 9. The plot shows that the improvement due to higher spectral resolution will allow to detect unblended water transitions with larger line/continuum ratio. The resolution of JWST/MIRI will improve the detection rate, but the gain is potentially still too low for Herbig stars, and higher resolution ($R \gg 3000$) is needed. The comparison between Herbig and T Tauri disks shows that the features are stronger for the earlier type objects (see Fig. 3), but the lines are also buried in a stronger continuum. The related stronger noise then makes the water lines even more difficult to be detected for Herbig PMS stars. T Tauri disks show weaker water line fluxes, but the lower continuum translates into a lower noise and so into a higher detection rate. This is in agreement with the more successful detection of mid-IR water blends towards T Tauri stars (about 50%).

3.5. Near-IR ro-vibrational water lines

As sanity check of the quality of our models, we computed the predicted line flux for a ro-vibrational water transition at

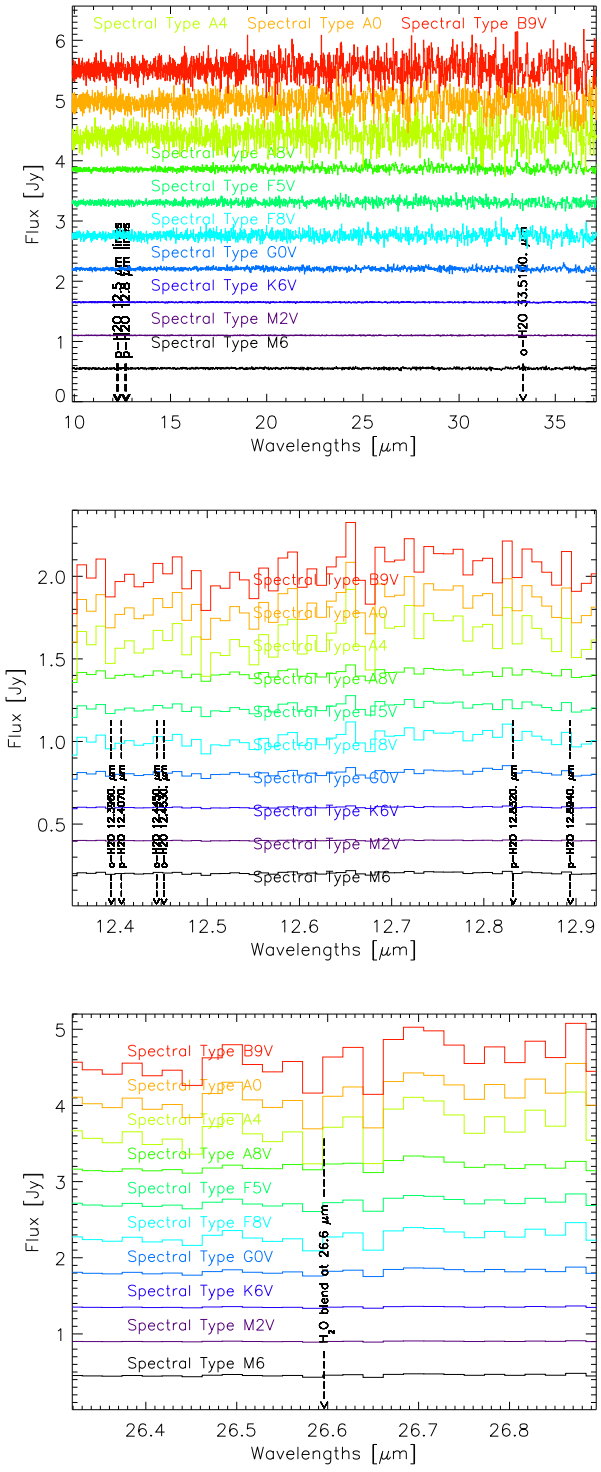

Fig. 8: Theoretical Spitzer SH/LH spectra ($R = 600$) for models with different central stars rebinned and noisy; full continuum subtracted spectrum, artificially shifted for all the models (top), zoom on the 12 μm region (middle), zoom on the 26.5 μm region (bottom).

2.934 μm (Fig. 10) targeted by Fedele et al. (2011). Our models, in agreement with the observations, predict that this ro-vibrational line should be undetectable in both T Tauri and Herbig star disks, due to sensitivity limits of the CRIRES spectrograph on the VLT (Kaeufl et al., 2004).

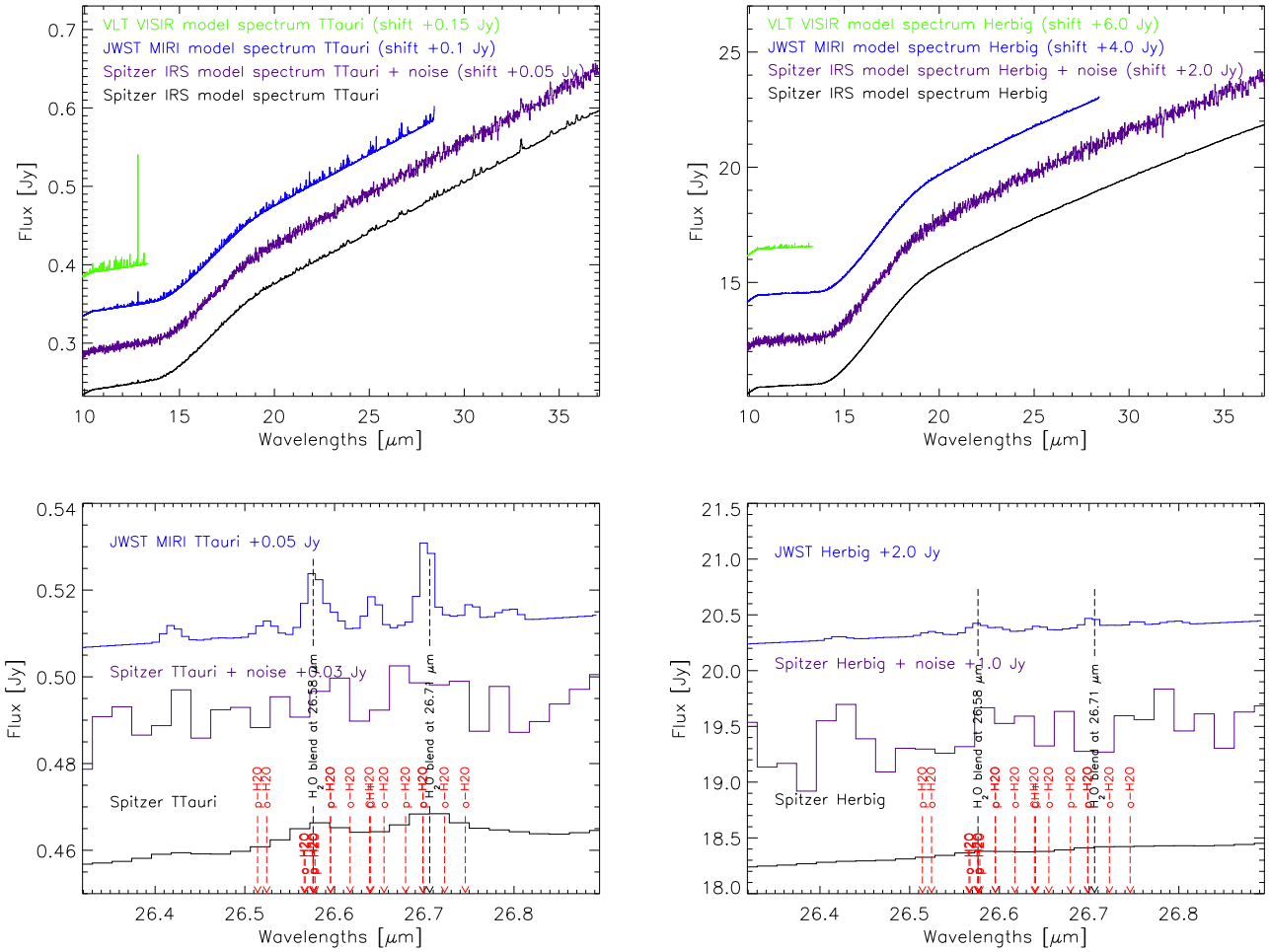
VLT VISIR model spectrum TTauri (shift +0.15 Jy)
JWST MIRI model spectrum TTauri (shift +0.1 Jy)
Spitzer IRS model spectrum TTauri + noise (shift +0.05 Jy)
Spitzer IRS model spectrum TTauri
Flux [Jy]
Wavelengths [μm]
VLT VISIR model spectrum Herbig (shift +6.0 Jy)
JWST MIRI model spectrum Herbig (shift +4.0 Jy)
Spitzer IRS model spectrum Herbig + noise (shift +2.0 Jy)
Spitzer IRS model spectrum Herbig
JWST MIRI TTauri +0.05 Jy
Spitzer TTauri + noise +0.03 Jy
Spitzer TTauri
H2O blend at 26.58 μm
H2O blend at 26.71 μm
JWST Herbig +2.0 Jy
Spitzer Herbig + noise +1.0 Jy
Spitzer Herbig

Fig. 9: Theoretical spectra convolved and re-binned at different resolutions (Spitzer IRS, R = 600; JWST MIRI, R = 3000 at 5.5 μm; VLT VISIR, R = 25000), and zoom in the 26 μm region. The ranges adopted are the same as the instruments spectrographs. VISIR is ground based, and the main limits is due to atmospheric transmission, we plotted only the region in which the transmissivity is $\geq$ 80%. The Spitzer spectrum with noise is also plotted in magenta. The strong feature at 12.93 μm in the VISIR modeled spectrum of a T Tauri star disk is due to H_2 ($J = 7-6$, $v = 0$). Water lines contributing to the blends at 26 μm are marked as vertical red arrows.

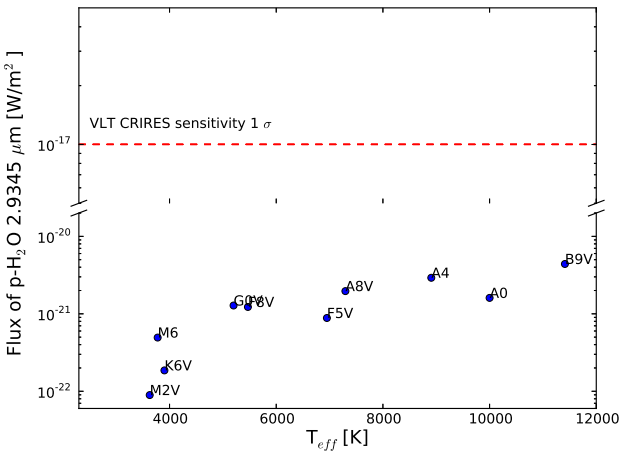

Fig. 10: p-H_2O 2.394 μm ro-vibrational line prediction from models with different central star. Typical sensitivity limits from the observations in Fedele et al. (2011) (10-40 minutes exposure) are marked as red dashed line.

4. Discussion

In this work, we investigate a couple of explanations for the non detection of mid-IR water towards more massive PMSs, based on our modeling physics and capabilities. The real disks can be more complex than the parametrized models studied here. In the following subsections, we will address individually the possible explanations for the low water detection rate in Spitzer spectra of Herbig stars.

4.1. Modeling assumptions

We consider here parametrized disk structures with monotonic shape and radial mass distribution. Several previous studies pointed out that the stronger irradiation from a hotter central star should produce a puffed-up inner disk (e.g. Dullemond, 2002). Observations towards some Herbig stars disks suggests that this scenario could be common (e.g. HD 163296, HD 141569A, and HD 150193A; Garufi et al., 2014b). This change in the inner disk is able to cast a strong shadows, but apparently from hydrostatic modeling it is not enough to produce lower temperatures

in the inner few au (Meijerink et al., 2012), and so mid-IR line fluxes should not be affected.

Our code is able to compute hydrostatic equilibrium disks, but we are limited by the heating/cooling processes implemented and the results tend towards a maximum flaring angle (Meijerink et al., 2012), which is generally not seen in detailed fitting results of individual objects (e.g. Tilling et al., 2012; Garufi et al., 2014a). The hydrostatic assumption itself is a limitation since it suppresses winds in disks, and this aspect is in conflict with the theory on photoevaporation (e.g. Hollenbach et al., 1994).

The rockline displacement in disks around bright PMSs, is not large enough to explain the water non detections. Our models suggest that in order to suppress the mid-IR water spectra, it is necessary to open a gap larger than 20 au or to lower the disk scale height below 10^{-3} au in the inner disk within 0.5 AU. From a recent near-IR interferometry survey of Herbig stars, about 5% of the objects are consistent with a gap larger than 20 au (Menu et al., 2015).

4.2. Intrinsic disk physics

Following the outcome of the first series of models, we performed a parameter space exploration to understand if physical differences between low and high mass PMSs disks could be a candidate explanation for the non detections. We found that indeed several properties are able to suppress the mid-IR water lines below the typical sensitivity range we considered (8×10^{-17}-8×10^{-18} W/m^2): very low disk scale height, large gaps (see previous Section), and high dust opacity (due to high dust content or grain size). These results are in agreement with our previous results on T Tauri stars.

Then also the standard model we took as fiducial case of a typical disk surrounding an Herbig star, is very close to the sensitivity range. The observations of Herbig stars overplotted on the parameter space explored, shows that disks populate largely the region we explore, and several objects could have been in principle detected only if they were close enough. In Pontoppidan et al. (2010a) we found that many of these targets were at distances larger than 220 pc. Again our model seems consistent with the observations.From our results, we are not able to exclude intrinsic differences in disks around Herbig stars with respect lower mass PMS stars. However, observations from Acke et al. (2009) conclude that 50% of the Herbig stars analyzed show scale heights enlarged by a factor 2 or 3 with respect hydrostatic prediction. This strongly puffed up inner region is able to cast a shadow that makes the disk cooler, as for HD 95881 (Verhoeff et al., 2010), possibly also for HD 144432 (Chen et al., 2012), and finally HD 163296 and HD 150193A (Garufi et al., 2014b). Then recent continuum radiative transfer modeling suggests that the mid-IR emitting regions of disks around different PMS stars (spanning from Brown dwarfs through Herbigs) are self-similar, in surface density, vertical distribution of dust and gas, and grain size distribution (Mulders & Dominik, 2012).

4.3. Instrumental noise

Finally we take into account the instrumental noise, that is able to affect relevantly the detection rate towards bright PMSs disks. Our study suggests that the low resolution and sensitivity of Spitzer IRS is the main cause of mid-IR water non detections in disks around Herbig stars. Mid-IR lines are buried in a stronger continuum, and the corresponding larger noise. We consider here a linear relation between noise and continuum, that is a conservative criterium. Pattern-noise and fringing[3] produce systematically stronger noise at high signal levels (i.e. for stronger continuum, Fig. 11). This noise can be reduced adopting deeper integration or multiple integration cycles. The observations analysed in Pontoppidan et al. (2010a) were deep enough for a relevant number of T Tauri stars, but not for Herbig stars.

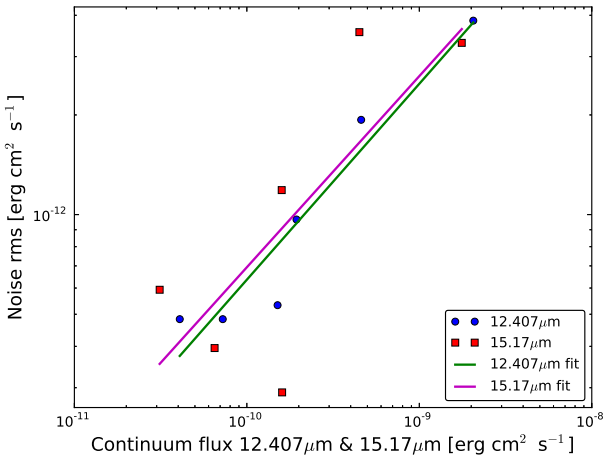

Fig. 11: Noise level versus continuum flux at the wavelengths of 12.407 μm (blue dots) and 15.17 μm (red squares). Overplotted are the fit to the data, green for 12.407 μm and magenta for the 15.17 μm.

Higher spectral resolution is needed to investigate water and likely other weaker mid-IR lines in disks around early type PMS stars, overcoming noise and integration time problems. JWST/MIRI would unblend already several Spitzer water lines, and will allow a better line/continuum ratio, but this could still be not high enough for Herbig stars. Ground based facilities, with spectral resolution > 20000 (like VISIR on VLT), are needed to improve the detection of water towards a wider sample of Herbig stars. However, ground-based observations will always be limited in wavelength coverage (and excitation temperatures) due to atmospheric transmission and telluric lines, and would limit the detections to some energetic rotational transitions as the 12.4 μm blend observed in Pontoppidan et al. (2010a).

5. Conclusions

From the outcome of our model we provide a scenario that can explain the observations in the mid-IR towards Herbig star: we considered some limitations in our description of disks around Herbig stars, and we think that these would not be problematic for the correct physical description of the mid-IR spectroscopy. Observations have been performed up to now with facilities affected by low spectral resolution and lower sensitivity. These two elements limit any possible firm conclusion about the nature of disks around Herbig stars, that can be intrinsically different from the ones surrounding T Tauri stars. Low S/N is the most likely explanation for the low detection rates of mid-IR water lines around early type PMSs. This problem affects also partially later type PMSs: T Tauri stars spectra are less noisy, however, mid-IR water line fluxes are lower, and the detection rate is only

[3] http://irsa.ipac.caltech.edu/data/SPITZER/docs/irs/features/

a factor two larger than for Herbig stars. Better performing instruments, with resolution > 3000 and longer integration times, are definitively needed to detect water successfully in the range 1-20 μm in protoplanetary disks.

Acknowledgements. The research leading to these results has received funding from the European Union Seventh Framework Programme FP7-2011 under grant agreement no 284405

References

Acke, B., Min, M., van den Ancker, M. E., et al. 2009, A&A, 502, L17
Antonellini, S., Kamp, I., Riviere-Marichalar, P., et al. 2015, A&A, 582, A105
Ardila, D. R., Golimowski, D. A., Krist, J. E., et al. 2007, ApJ, 665, 512
Aresu, G., Kamp, I., Meijerink, R., et al. 2011, A&A, 526, A163
Aresu, G., Meijerink, R., Kamp, I., et al. 2012, A&A, 547, A69
Banzatti, A., Meyer, M. R., Bruderer, S., et al. 2012, ApJ, 745, 90
Barber, R. J., Tennyson, J., Harris, G. J., & Tolchenov, R. N. 2006, MNRAS, 368, 1087
Bergin, E. A., Hogerheijde, M. R., Brinch, C., et al. 2010, A&A, 521, L33
Bertout, C., Siess, L., & Cabrit, S. 2007, A&A, 473, L21
Carmona, A., Pinte, C., Thi, W. F., et al. 2014, A&A, 567, A51
Carr, J. S. & Najita, J. R. 2008, Science, 319, 1504
Chen, L., Kreplin, A., Wang, Y., et al. 2012, A&A, 541, A104
Clampin, M. 2011, in Society of Photo-Optical Instrumentation Engineers (SPIE) Conference Series, Vol. 8146, Society of Photo-Optical Instrumentation Engineers (SPIE) Conference Series
Donati, J.-F., Gregory, S. G., Alencar, S. H. P., et al. 2013, MNRAS, 436, 881
Draine, B. T. & Lee, H. M. 1984, ApJ, 285, 89
Du, F. & Bergin, E. A. 2014, ApJ, 792, 2
Dubrulle, B., Morfill, G., & Sterzik, M. 1995, Icarus, 114, 237
Dullemond, C. P. 2002, A&A, 395, 853
Ellerbroek, L. E., Podio, L., Dougados, C., et al. 2014, A&A, 563, A87
Fedele, D., Bruderer, S., van Dishoeck, E. F., et al. 2013, A&A, 559, A77
Fedele, D., Bruderer, S., van Dishoeck, E. F., et al. 2012, A&A, 544, L9
Fedele, D., Pascucci, I., Brittain, S., et al. 2011, ApJ, 732, 106
Garcia Lopez, R., Natta, A., Testi, L., & Habart, E. 2006, A&A, 459, 837
Garufi, A., Podio, L., Kamp, I., et al. 2014a, A&A, 567, A141
Garufi, A., Quanz, S. P., Schmid, H. M., et al. 2014b, A&A, 568, A40
Hartigan, P., Edwards, S., & Ghandour, L. 1995, ApJ, 452, 736
Hogerheijde, M. R., Bergin, E. A., Brinch, C., et al. 2011, Science, 334, 338
Hollenbach, D., Johnstone, D., Lizano, S., & Shu, F. 1994, ApJ, 428, 654
Houck, J. R., Roellig, T. L., van Cleve, J., et al. 2004, ApJS, 154, 18
Husser, T.-O., Wende-von Berg, S., Dreizler, S., et al. 2013, A&A, 553, A6
Kaeufl, H.-U., Ballester, P., Biereichel, P., et al. 2004, in Society of Photo-Optical Instrumentation Engineers (SPIE) Conference Series, Vol. 5492, Ground-based Instrumentation for Astronomy, ed. A. F. M. Moorwood & M. Iye, 1218–1227
Kamp, I., Tilling, I., Woitke, P., Thi, W.-F., & Hogerheijde, M. 2010, A&A, 510, A18
Kessler, M. F., Steinz, J. A., Anderegg, M. E., et al. 1996, A&A, 315, L27
Lagage, P.-O., Durand, G. A., Lyraud, C., et al. 2000, in Society of Photo-Optical Instrumentation Engineers (SPIE) Conference Series, Vol. 4008, Optical and IR Telescope Instrumentation and Detectors, ed. M. Iye & A. F. Moorwood, 1120–1131
Lahuis, F. 2007, PhD thesis, Leiden Observatory, Leiden University, P.O. Box 9513, 2300 RA Leiden, The Netherlands
Lahuis, F. & Boogert, A. 2003, in SFChem 2002: Chemistry as a Diagnostic of Star Formation, proceedings of a conference held August 21-23, 2002 at University of Waterloo, Waterloo, Ontario, Canada N2L 3G1. Edited by Charles L. Curry and Michel Fich. NRC Press, Ottawa, Canada, 2003, p. 335., ed. C. L. Curry & M. Fich, 335
Lahuis, F., van Dishoeck, E. F., Blake, G. A., et al. 2007, ApJ, 665, 492
Liskowsky, J. P., Brittain, S. D., Najita, J. R., et al. 2012, ApJ, 760, 153
López-Martínez, F. & Gómez de Castro, A. I. 2014, MNRAS, 442, 2951
Luhman, K. L., Allen, P. R., Espaillat, C., Hartmann, L., & Calvet, N. 2010, ApJS, 186, 111
Maaskant, K. M., Min, M., Waters, L. B. F. M., & Tielens, A. G. G. M. 2014, A&A, 563, A78
Mandell, A. M., Mumma, M. J., Blake, G. A., et al. 2008, ApJ, 681, L25
Manset, N., Bastien, P., Ménard, F., et al. 2009, A&A, 499, 137
McJunkin, M., France, K., Schneider, P. C., et al. 2014, ApJ, 780, 150
Meeus, G., Montesinos, B., Mendigutía, I., et al. 2012, A&A, 544, A78
Meijerink, R., Aresu, G., Kamp, I., et al. 2012, A&A, 547, A68
Meijerink, R., Pontoppidan, K. M., Blake, G. A., Poelman, D. R., & Dullemond, C. P. 2009, ApJ, 704, 1471
Menu, J., van Boekel, R., Henning, T., et al. 2015, ArXiv e-prints
Min, M., Dullemond, C. P., Kama, M., & Dominik, C. 2011, Icarus, 212, 416
Mulders, G. D. & Dominik, C. 2012, A&A, 539, A9
Müller, A., van den Ancker, M. E., Launhardt, R., et al. 2011, A&A, 530, A85
Murphy, T. & Meiksin, A. 2004, MNRAS, 351, 1430
Perryman, M. A. C., Lindegren, L., Kovalevsky, J., et al. 1997, A&A, 323, L49
Pontoppidan, K. M., Salyk, C., Blake, G. A., & Käufl, H. U. 2010a, ApJ, 722, L173
Pontoppidan, K. M., Salyk, C., Blake, G. A., et al. 2010b, ApJ, 720, 887
Riviere-Marichalar, P., Ménard, F., Thi, W. F., et al. 2012, A&A, 538, L3
Salyk, C., Blake, G. A., Boogert, A. C. A., & Brown, J. M. 2009, ApJ, 699, 330
Salyk, C., Pontoppidan, K. M., Blake, G. A., et al. 2008, ApJ, 676, L49
Siess, L., Forestini, M., & Bertout, C. 1999, A&A, 342, 480
Tennyson, J., Zobov, N. F., Williamson, R., Polyansky, O. L., & Bernath, P. F. 2001, Journal of Physical and Chemical Reference Data, 30, 735
Tilling, I., Woitke, P., Meeus, G., et al. 2012, A&A, 538, A20
van Boekel, R., Min, M., Waters, L. B. F. M., et al. 2005, A&A, 437, 189
van den Ancker, M. E., The, P. S., Tjin A Djie, H. R. E., et al. 1997, A&A, 324, L33
van Dishoeck, E. F., Bergin, E. A., Lis, D. C., & Lunine, J. I. 2014, Protostars and Planets VI, 835
van Leeuwen, F., ed. 2007, Astrophysics and Space Science Library, Vol. 350, Hipparcos, the New Reduction of the Raw Data
Verhoeff, A. P., Min, M., Acke, B., et al. 2010, A&A, 516, A48
Woitke, P., Kamp, I., & Thi, W.-F. 2009, A&A, 501, 383
Woitke, P., Riaz, B., Duchêne, G., et al. 2011, A&A, 534, A44

Appendix A: Sensitivity limits

Our analysis sample includes a selection of T Tauri and Herbig Spitzer-IRS high resolution observations. BCD data products were retrieved from the Spitzer archive[4]. The data were reduced with the c2d IRS science pipeline using the PSF extraction method (see Lahuis et al., 2007; Lahuis, 2007, for details), which provides higher S/N spectra then the standard tapered aperture extraction used to populate the Spitzer archive. After extraction, additional defringing (Lahuis & Boogert, 2003) was applied to remove any low-level fringe residuals.

Sensitivity limits were determined by calculating the line flux for synthetic lines with an amplitude equivalent to the 1-σ noise level in the IRS spectrum at the respective blend wavelengths and a width comparable to the blend width at a spectral resolution of 600.

Appendix B: Spectral convolution

We applied Gaussian convolution and rebinning to the theoretical spectra from our models. For this task we used the ISO spectral analysis package (Kessler et al., 1996), considering the three resolutions of Spitzer IRS LH/SH modules (R = 600; Houck et al., 2004), VLT VISIR (R = 25000; Lagage et al., 2000). For JWST MIRI we split the range in four spectral windows: R = 2800 for 7.63-11.71 μm, R = 2500 for 11.71-13.59 μm, R = 2300 for 13.59-18.14 μm, R = 1600 for 18.14-28.43 μm, accounting for the variable spectral resolution (Clampin, 2011). We add noise through a random generator according to

$$N = F_{\rm cont} \cdot \frac{U([0,1])}{100} \tag{B.1}$$

N is the computed noise, it is a function of the continuum flux ($F_{\rm cont}$) multiplied for a random generator between 0 and 1 ($U([0,1])$), and of the selected S/N ratio, here we consider 100 as claimed in Pontoppidan et al. (2010a).

[4] http://irsa.ipac.caltech.edu/data/SPITZER/docs/spitzerdataarchives/

Appendix C: Far UV spectra

FUV data are produced combining observations from IUE, FUSE, HST/STIS, HST/COS and when available HST/ACS archival data (Fig. C.1). These data have been taken in multiple observations of the same objects, and have different resolution, integration time, spectral range and noise. Due to the complex dataset, the best spectra we use is an average performed through a sophisticated procedure described in detail in Dionatos et al in prep.

Table C.1: Far UV spectra data source, and number of epochs for each source.

Star	IUE	FUSE	STIS	COS	ACS
HD 100546	9	6	8	0	0
HD 97048	12	0	0	0	0
HD 163296	31	6	8	0	0
HD 142666	7	2	0	0	0
HD 135344B	0	2	0	8	0
RY Tau	107	0	6	0	1
RY Lup	4	0	4	0	1
DN Tau	19	0	0	0	1
CY Tau	0	0	5	0	2
DO Tau	0	0	0	0	1

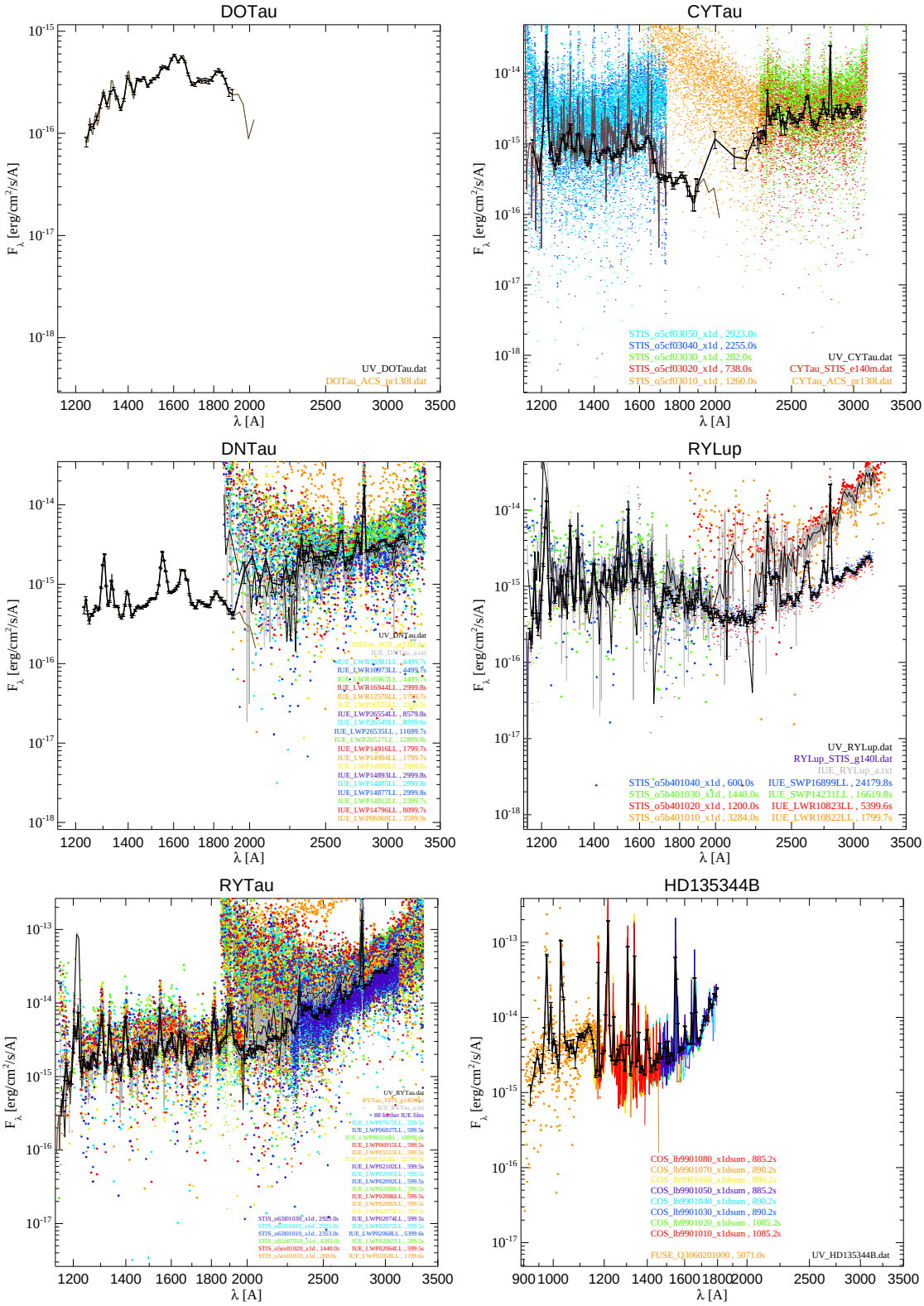

Fig. C.1: Far UV component for each of the stars we modeled. The black line is the best fit of the multiple epochs of observations. Spectra data points are color coded, and the original files are labeled.

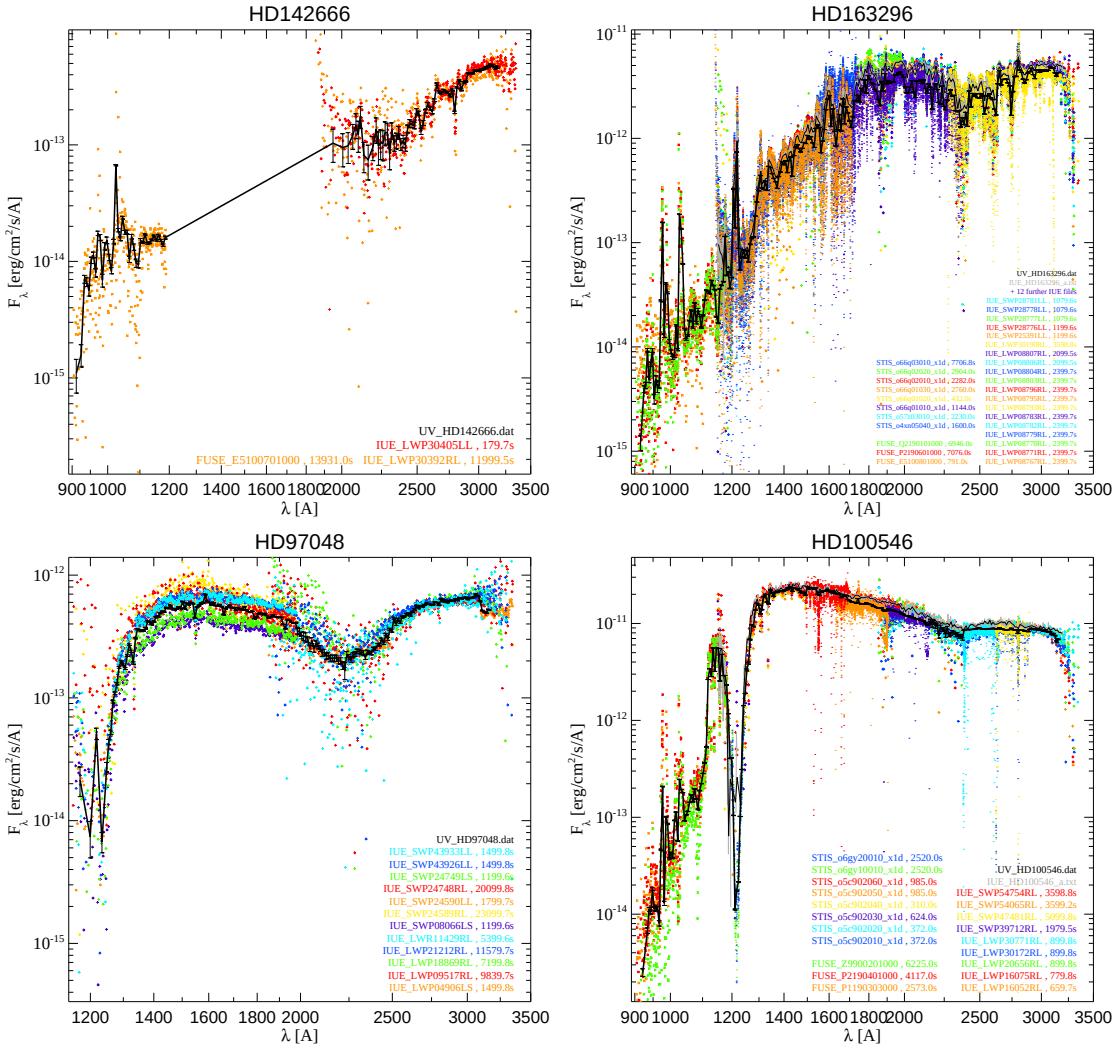

Fig. **??** Continued.